

Base Course Geocell Reinforcement Evaluation by comparing 3-D FEM and Laboratory Evaluation

S. Inti¹, M. Sharma¹, C. Tirado¹ and V. Tandon^{1*}

¹The University of Texas at El Paso, El Paso, Texas, United States of America

*E-Mail: Corresponding vivek@utep.com, TP: +19157476924

Abstract: The shortage of high-grade base material and emphasis on using recycling base material has led to use of geocells reinforced bases in the past decade. The geocells provide reinforcement by confining base material and have been used for increasing bearing capacity of supporting soil, reducing settlements, using inferior quality material, reducing thickness of base layers, etc. It can be an economical option in rehabilitation of pavements and construction of low volume roads. Various studies have been conducted to evaluate the behaviour of geocell reinforced layers using expensive and time intensive laboratory tests. The working principle of geocell reinforced layers using various pavement materials, loading types, geocell types etc., can be comprehended quickly and economically using Finite Element Modelling (FEM). In this study, various significant FEM model parameters like constitutive material models and contact models were examined. The results were compared with the laboratory test results and specific contact and constitutive material models that predict behaviour similar to the laboratory results were recommended.

Keywords: Geocell, Finite Element Modelling (FEM), Contact models, Constitutive models.

1. Introduction

Geocells are honeycomb interconnected cells that completely encase the soil and provide three-dimensional confinement geometry, which reduces the lateral movement of the soil particles [1]. Due to confinement, the geocells increase the stiffness and the load-deformation behavior of the base layers; thus, reducing the deformation of the soil. The soil-geocell layers act as a stiff mat, distributing the vertical traffic loads over a much larger area of the subgrade soil [1]; thus, increasing load bearing capacity of subgrade layer. Although, geocells have been used and studied [1, 2, 3, and 4] the mechanism for improved bearing capacity and benefits of using geocell have not been well understood. In addition, the influence of in-fill material quality on performance of geocells has not been evaluated which is a critical issue when only lower/marginal quality material is available.

Earlier research (both laboratory and finite element) on Geocell was focused more on structure foundation (mostly building foundations) and less attention was disbursed towards geocell use in pavements. Since the loading pattern differs from buildings to pavements, the research findings from structures may not be applicable to pavements. While numerical modelling, many researchers modeled the geocell and infill material as a

composite material [5, 6, 7, and 8] using finite element or finite difference methods but very few have modeled them as a separate material [9, 10, 11, and 12]. In geocell reinforced base layer, the infill material (linear elastic plastic) and geocell (elastic) responds simultaneously to loading, but the working mechanism of each material is different. In order to model geocell reinforced base layer more precisely, the behavior of each material (infill and geocell) needs to be evaluated separately. In this study, the geocell and infill material were modelled separately. The focus of the study is to evaluate various parameters like constitutive material models, contact models, and various material types.

2. Methodology

Modeling of the geocells and infill material was performed using finite element software LS-Dyna. A three layered pavement structure as shown in Figure 1 was modeled with a subgrade, geocell-reinforced base layer, and a top un-reinforced base layer. Geocell panels were modeled as a shell element of rhomboidal shape that closely resembles the curve shape of the honeycomb structure. The Belytschko-Lin-Tsay Shell (BLT) formulation was selected for modeling the geocell. The BLT element formulation is suitable for four node (quad) shell elements, and offer a single point

integration with hourglass control. Each element has six global degrees of freedom per node (i.e., d_x , d_y , d_z , r_x , r_y , r_z), and five (through thickness) integration points [13]. In addition, they have a bi-linear nodal interpolation.

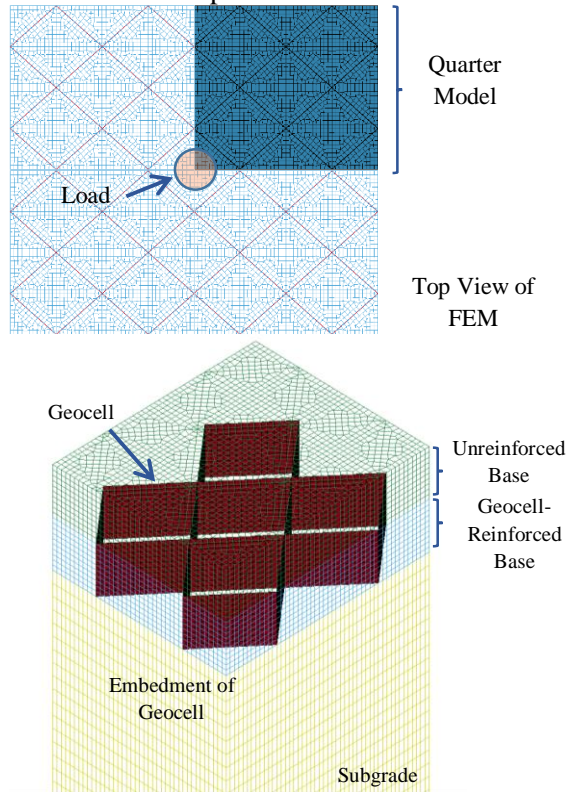


Figure 1: Finite element model of pavement structure

The 8-node constant stress solid elements were selected for the modeling of the base and subgrade structures. These solid elements use one-point integration and hourglass control. Considering the lattice pattern of geocell and its soil embedment in the base layer, proper element arrangement and nodal connectivity is required to adjust to the geocell lattice pattern and to avoid any penetration of nodes between the two different materials parts. The resulting mesh consisted of quad elements representing the geocell and a mix of solid hexahedral and prisms elements for the soil. To reduce the number of elements, and consequently the execution time, a quarter model was used.

3. Pavement Structure Dimensions and Finite Element Model Properties

Table 1 summarizes the dimension of the FEM quarter model. The applied boundary conditions restricted the displacement in the direction orthogonal to the planes. The geocell-reinforced base layer was unrestrained at the end to allow

lateral movement to simulate field conditions where shoulder is not attached to the pavement.

3.1 Geocell Dimensions and Properties

Geocell dimensions and the properties used in the analyses are shown in Table 2. The properties shown correspond to a Presto GW20V geocell type, which was one of the geocells evaluated in the laboratory and modeled as linear elastic material.

Table 1: Dimensions of FEM quarter model

Pavement Structure Thickness		
Layers	Geocell Reinforced Pavement Structure	Unreinforced Pavement Structure
Top Base	100 mm	100 mm
Geocell Reinforced Base	100 mm	100 mm
Subgrade	1000 mm	1000 mm
Finite Element Model Size (Quarter Model)		
Longitudinal Dimension, x -axis	450 mm	
Transversal Dimension, y -axis	400 mm	

Table 2: Geocell dimensions and properties

Geocell Dimensions (Presto GW20V)	
Longitudinal Length	234 mm
Transversal Length	200 mm
Height	100 mm
Thickness	1 mm
Material Properties	
Density	950 kg/m ³
Transversal Length	414 MPa
Poisson's Ratio	0.45

3.2 Loading Conditions

In this study, a haversine cyclic load was applied at the center of the geocell using 150 mm diameter plate. Figure 2 shows the applied load consisting of multiple cycles each with a loading period of 0.1 sec and a rest period of 0.9 sec. The magnitude of the repeated peak load was maintained at 550 kPa, which is equivalent to tire pressure.

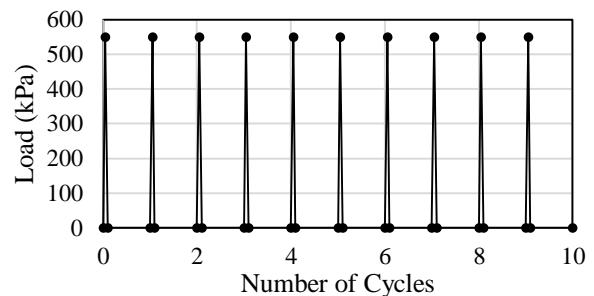


Figure 2: Loading cycle

3.3 Soil Material Model and Properties

In this study, three different constitutive material models were evaluated: linear elastic, Mohr Coulomb and FHWA soil model. FHWA soil model is a modified Mohr-Coulomb model available in LS-DYNA [14] extended to include excess pore-water effects, strain softening, strain hardening, strain-rate effects and elements deletion. These enhancements to the standard soil material models were made to increase the accuracy, robustness, and ease of use for roadside safety applications [14].

The yield surface for the FHWA soil model is given by [14]:

$$F = -P \sin \varphi + \sqrt{J_2 K(\theta)^2 + Ahyp^2 \sin^2 \varphi} - c \cos \varphi = 0 \quad (1)$$

where:

P = pressure,

φ = internal friction angle,

J_2 = second invariant of the stress deviator,

c = cohesion,

$Ahyp$ = Drucker-Prager hyperbolic coefficient parameter approximated by

$$Ahyp = \frac{c}{20} \cot(\varphi), \text{ and} \quad (2)$$

$K(\theta)$ = Klisinski [15] modified Mohr-Coulomb function of angle θ in deviatoric plane, defined as

$$K(\theta) = \frac{4(1-e^2)\cos^2\theta + (2e-1)^2}{2(1-e^2)\cos\theta + (2e-1)\sqrt{4(1-e^2)\cos^2\theta + 5e^2 - 4e}} \quad (3)$$

where e is an eccentricity parameter describing the ratio of triaxial extension strength to triaxial compression strength responsible for third invariant (J_3) effects, ranging $0.5 < e \leq 1.0$, and initially modelled as $e = 0.7$, and angle θ obtained from

$$\cos 3\theta = \frac{3\sqrt{3}J_3}{2\sqrt{J_2^3}} \quad (4)$$

The modified yield surface, as shown in Figure 3, is a hyperbola fitted to the Mohr-Coulomb surface. At the crossing of the pressure axis (zero shear strength), the modified surface is a smooth surface and it is perpendicular to the pressure axis.

4 Contact Model

One of the most important aspects for understanding the behavior of geocell-reinforced pavements comes from the interaction between the geocell and the surrounding geomaterials. In the case of composite, the modelling of geocell reinforcement becomes significantly simplified when a fully bonded model is considered. In a

fully bonded model, shell nodes belonging to the geocell reinforcement are shared with solid elements representing the host infill base material. Thus, the solid elements (i.e. the base material) constrains the translational degrees of freedom of the embedded geocell. This approach has been followed by Bortz and Hossain [12] using geocell modeled as shell in an embedded region. Other authors have preferred to include an interface shear stress strain relationship based on Mohr Coulomb sliding criterion [10, 16, and 17]. The advantages offered by this type of interface consists on faster execution times and somewhat simplified meshing.

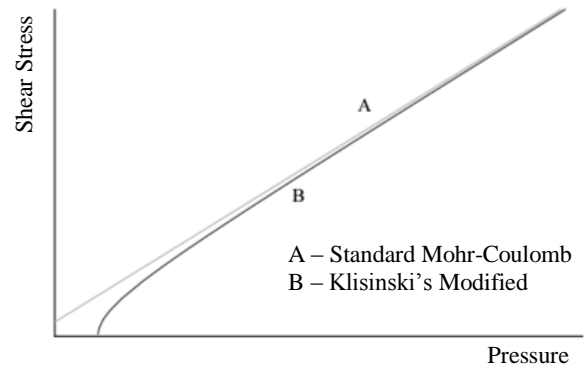


Figure 3: Comparison of Mohr-Coulomb yield surfaces in shear stress-pressure space [14].

To permit sliding between the soil and geocell, a contact models needs to be considered. Its implementation requires additional meshing and requires longer computational time. Leshchinsky and Ling studied the effects of geocell confinement on ballasted embankments by modelling the interaction of geocell and embankment with contact elements having “hard” normal contact (no penetration) and tangential contact was modeled as $2/3$ of the tangent of the friction angle (45°), applied using penalty friction algorithm [18]. In this study, different contact models were evaluated and compared to a geocell-reinforced fully bonded model and to an unreinforced (continuum) model. Among the evaluated contact models, the LS-DYNA automatic single surface contact model and a discrete-beam element interface were found to be the most promising for best modelling the soil-geocell interaction.

4.1 Automatic Single Surface Contact

LS-DYNA automatic contact types determine the contact surfaces by projecting normally from the shell mid-plane a distance equal to one-half the contact thickness [13]. For single surface contacts, slave surface is typically defined as a list of parts while no master surface is defined. The automatic

single surface contact makes use of a penalty method consisting in checking slave nodes penetrating the master surface. An interface force is applied between the slave node n_i and its contact point if penetration occurs, emulating the addition of an interface spring. Stiffness k_i for master segment s_i is defined as

$$k_i = \frac{f_{si} K_i A_i^2}{V_i} \text{ for brick elements, and} \quad (5)$$

$$k_i = \frac{f_{si} K_i A_i}{\max(l_{diag})} \text{ for shell elements,} \quad (6)$$

where K_i is bulk modulus, V_i is volume, A_i is face area of the element in s_i , l_{diag} is the shell diagonal length, and f_{si} is a scale factor for the interface stiffness (normally $f_{si} = 0.10$) [13].

Friction is based on a Coulomb formulation. The model implements a friction algorithm that makes use of an elastic plastic spring. The algorithm is based on an iterative process that starts by calculating the yield force based on the friction and the normal force, followed by the calculation of the incremental movement of the slave node to update the interface force and check yield condition. An exponential interpolation function smooths the transition between the static and dynamic coefficients of friction based on the relative velocity between the slave node and the master, as described in the LS-DYNA theory manual [13].

4.2 Discrete Beam Element Interface

The use of discrete beam element for establishing a geocell-soil interface was also considered. Through these means, discrete beams were used to connect geocell nodes to solid nodes. A discrete beam has up to 6 degrees of freedom (DOF) whereas a spring has only one DOF. Resultant forces and moments of a discrete beam are output in the local (r, s, t) coordinate system. The length of a discrete beam may be zero or nonzero. In this study, discrete elements with linear elastic relations were used.

5. Results and Discussion

5.1 Evaluation of Material Model

For evaluating the material model, studies were carried first using fully bonded models followed by the inclusion of geocell reinforcement using LS-DYNA automatic contact model. Results shown in this section correspond to the latter model. Initially, the base and subgrade layers were modeled as linear elastic materials and soil

properties used in the analysis are shown in Table 3 [19].

Only one loading cycle was attempted in the linear elastic FE analysis as other cycles would yield identical results because no plastic deformation is expected in an elastic material. The load cycle consisted of a loading period of 0.1 sec and a rest period of 0.9 sec, with a peak pressure of 550 kPa. Analysis was done for both reinforced and unreinforced pavement section and the responses were compared.

Table 2: Material properties of soil used in modelling [17]

Layer	Modulus (MPa)	Cohesion (kN/m ²)	Friction Angle, ϕ	Unit Weight (kN/m ³)
Subgrade 1 (Clay)	12	10.0	15°	15.8
Subgrade 2 (Clay)	16	10.0	15°	15.0
Base 1 (Sand)	40	0.01	34°	20.0
Base 2 (Sand)	60	1.0	29°	19.5
Base 3 (Sand)	80	0.0	29°	20.0

No significant change in responses for unreinforced and reinforced was observed using linear elastic material model. The plot shown in Figure 4, for a 35 MPa base layer and 35 MPa subgrade, and 150 mm diameter load plate applying a pressure of 550 kPa at the center of the cell, shows no significant difference in terms of deflection with respect to depth. Similar responses were obtained for all other loading scenarios and pavement distresses.

In addition to no significant effect of the geocell reinforcement, this model does not take into account plastic deformation as observed in soils subjected to repeated loading. Thus, soils models that can predict elastic as well as plastic deformation were selected for evaluating response of geocell reinforcement.

Mohr-Coulomb is the most commonly used soil material model [6, 9, 10, and 20] that is able to address the soil's elastic as well as plastic behavior. Use of this model in LS-DYNA incurred in excessive deformation at the corners farther from the loaded section forcing the analysis to terminate after 10 cycles. This model was not found suitable as deformations seemed excessive when compared to other studies. To overcome this problem, the FHWA soil model was considered instead as this model also allows to accommodate permanent deformation.

Four different types of base materials were evaluated with two distinct types of subgrades, described in Table 3. Pavements were subjected to multiple cycles with constant peak pressure of 550 kPa, as shown in Figure 2. Figure 8 shows the deflection with respect to depth under the center of load occurring at the peak load of the first cycle for both reinforced and unreinforced base layers.

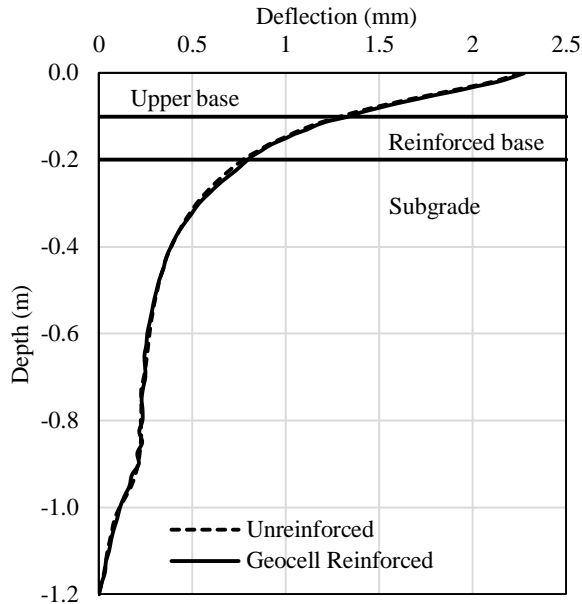


Figure 4: Change in vertical deflection with depth

The plots shown in Figure 5 correspond to the modeling of pavements consisting of Subgrade-1 (12 MPa) and Bases 1-3, ranging from 40 to 80 MPa (refer to Table 3). In these figures, it can be seen that geocell reinforcement reduces the surface deformation when compared to unreinforced sections. Yet, geocell reinforcement impact on surface deformation decreases as the base becomes more rigid. Figure 6 shows the decrease in surface deformation in terms of percent reduction between the unreinforced and reinforced sections with respect to base modulus. As the modulus of the base layer improves, the effect of geocell reinforcement diminishes. The benefit of using a geocell-reinforced base layer was not evident when a good base quality material was used.

5.2 Evaluation of Contact Model

For evaluating the contact model, the 3-D model was reduced to a one-thick element wide model as shown in Figure 7 to better focus on the behavior of the contact and expedite the analysis. Three cells are modelled, separated by the geocell material.

Both contact models were evaluated and compared with respect to the fully bonded model and to

unreinforced models, using the base material with $E = 120 \text{ MPa}$, $\nu = 0.33$, $c = 0$, $\phi = 26.8^\circ$ properties. Load was reduced pressure of 270 kPa, still applied to a 150 mm diameter load, and symmetry conditions were applied on left boundary to account for a half-model. Responses were evaluated the interface, at base mid-layer, on elements adjacent to both sides of the geocell, as indicated in Figure 7.

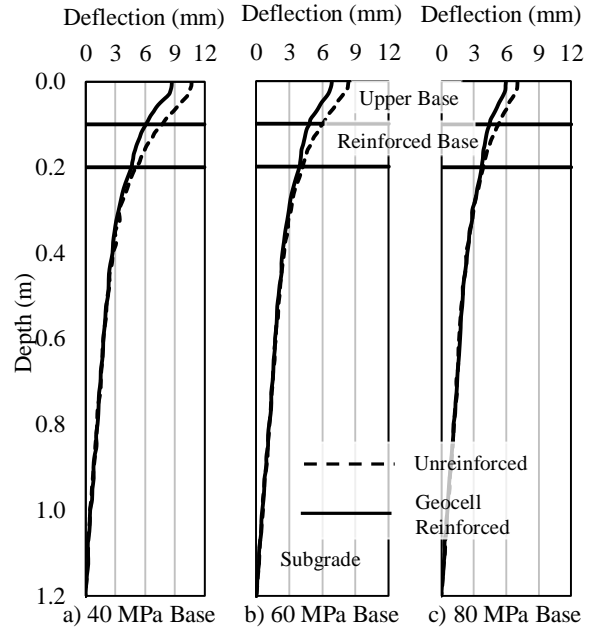


Figure 5: Vertical deflection with respect to depth at peak load of first cycle for a two-layer pavement system consisting of Subgrade-1 ($E=12 \text{ MPa}$, $\nu=0.33$, $c=10 \text{ kN/m}^2$, $\phi=15^\circ$) and different base properties.

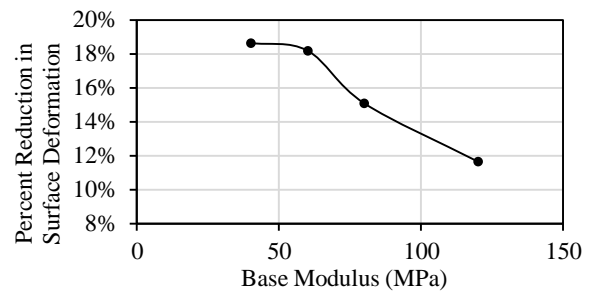


Figure 6: Percentage reduction in surface deformation with respect to base modulus for a pavement with Subgrade-1 ($E=12 \text{ MPa}$, $c=10 \text{ kN/m}^2$, $\phi=15^\circ$) material.



Figure 7: Reduced mesh for evaluation of contact interface.

For the automatic single contact model, it was observed that the model failed to recognize the adjacent base materials appropriately, and consequently, thin shells were replaced by thick shells, as the latter did perform satisfactorily with the contact model. All responses were evaluated, but particular emphasis was placed on the longitudinal stress to quantify reduction in stress transfer through the geocell material and the interface. In Table 3, the results from different cases are shown: (1) a linear elastic model based on the relationships developed by Boussinesq and implemented in BISAR, (2) an FE unreinforced model using FHWA soil model for the base material, (3) an unreinforced model with automatic surface to surface contact model to account for soil interaction, (4) a geocell-reinforced model with fully bonded conditions between geocell and soil, (5) a geocell-reinforced with automatic single surface model to provide contact between geocell (thick shell) and soil, and (6) and (7) an interface defined with springs (beam discrete elements with different properties) to allow interaction between soil and geocell.

Table 3: Reinforced base responses at mid-layer, adjacent to geocell, in terms of longitudinal stress

Contact	Soil Before Geocell	Soil After Geocell
Longitudinal stress σ_x (Pa)		
1. Linear Elastic*	38.6	34.0
2. FHWA Soil*	30.3	30.6
3. Aut. Surf. Contact Soil to Soil*	34.8	33.4
4. Fully Bonded	41.8	41.0
5. Aut. Single Surface**	30.7	29.5
6. Spring: $k_n=10$ kN/m, $k_s=1$ kN/m	6.2	6.0
7. Spring: $k_n=100$ kN/m, $k_s=1$ kN/m	24.1	24.5

* Unreinforced, ** Thick Shell

Based on the base material responses, among others not included in this paper for brevity, it was found that in the fully bounded model higher stresses developed compared to other models. Though not included in Table 3, contrary to the spring-connected interface, friction values on the automatic single surface model did not have a significant effect on the responses. When connected by means of discrete beams (springs), both thin shell and thick shell elements yielded very similar results, yet when the automatic single surface contact model was used with a thin shell, the stress was not transferred from one cell to the adjacent cell through the geocell, meaning that the search algorithm failed to establish a contact. This problem is overcome by using thick shell instead of thin shell elements (results shown in Table 3). In

addition, from the table it can be seen stress varies considerably in models with spring-connected interfaces depending on their normal and shear stiffness values. A drawback on the use of springs lies on the lack of standard laboratory test procedures for determining the normal and shear stiffness for these spring elements.

5.3 Laboratory evaluation of soil-geocell contact

An additional study was developed for evaluating the behavior of the soil-geocell interface. A single geocell performance was monitored during loading. A test was conducted in a 900 mm diameter cylindrical tank. A single geocell was placed on top of a 600 mm thick compacted subgrade and infill materials in the geocell pocket were compacted in three layers. A circular steel plate with 150 mm diameter and 20 mm thickness was placed at the center of the geocell pocket. The vertical load was applied through an MTS load frame and the settlement of plate was recorded. Strain gages were glued at the mid-height of the geocell, around the cell circumference, as shown in the Figure 8. A quarter bridge circuit arrangement was used to connect the strain gauges. Strain was recorded using LMS Scadas Mobile data acquisition system. A repeated load was applied in the middle of the cell as shown in the Figure 8.

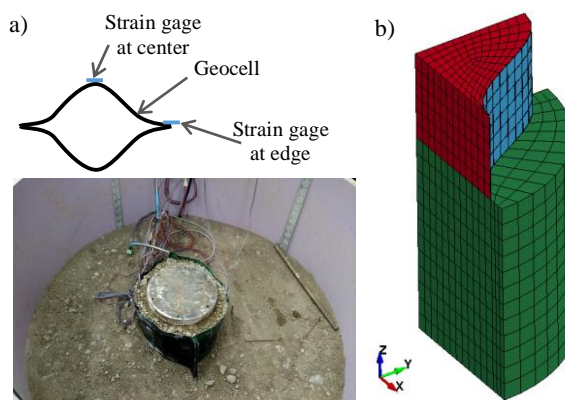


Figure 8: (a) Laboratory setup and (b) its numerical model

As per the laboratory test results, the hoop strains (circumferential strains) were maximum at the center and decreased towards the edge. Though the FEM results for both contact models provided similar results, the hoop strains at the edge of the geocell differed from the laboratory results, when an automatic single surface contact model is used. Hoop strains determined from the numerical model with a soil-geocell interface using discrete beam elements, i.e. 6-DOF spring elements, were closer to laboratory strain gage measurements, at the center and edge of the geocell, and along the

perimeter of the geocell, as well. As a result, the results shown in this section are for an FE model using discrete beam elements to provide contact between soil and geocell. Figures 9 and 10 show the hoop strains observed on the edge and the center of geocell, respectively, for 100 cycles, as obtained from laboratory test and FEM. It must be noted that the FE model captured data continuously for every cycle up to the 10th cycle; afterwards, responses are only shown for every 10 cycles.

The measured strains at the edge of geocell observed were in the range of 240 $\mu\epsilon$ up to 90 load cycles during loading and increased up to 300 $\mu\epsilon$ after 90 cycles. The FEM model generated strains in the range of 100-350 $\mu\epsilon$ during loading and 100 $\mu\epsilon$ during rest period. The key difference in the results were the elastic strain in the FEM model which were higher in comparison to laboratory results. The difference in responses could be attributed impossibility of achieving zero load during unloading in the lab testing for each cycle and geocell characterized as a perfect elastic material in the FE model. Similar behavior can be observed in the responses at the center of geocell.

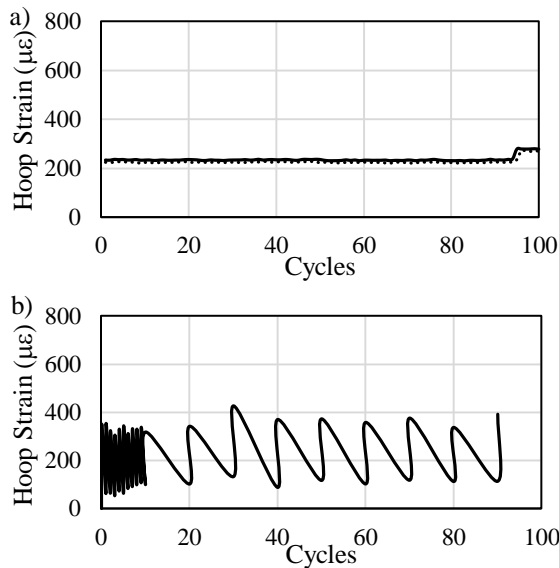


Figure 9: Strains at edge of geocell for a) laboratory b) FEM.

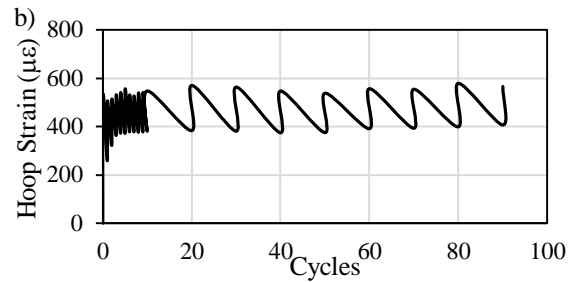
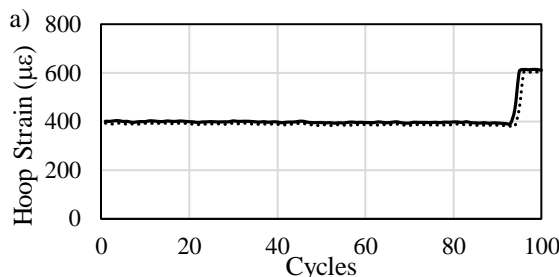


Figure 10: Strains at center of geocell for a) Laboratory, b) FEM.

6. Conclusions

Following conclusions are drawn from this study:

1. Modelling soil elements as a linear elastic shows no difference in the pavement responses for geocell reinforced pavements.
2. FHWA soil model behaves well compared to other material models and can be used for modelling soil.
3. Reinforcing the base layer with geocell reduces the permanent deformation and stresses in the pavements.
4. As the modulus of the base layer improves, the effect of geocell reinforcement diminishes.
5. The benefit of using a geocell-reinforced base layer was not evident when a good base quality material was used for FEM analysis.
6. LS-DYNA automatic contact models were found to have issues when establishing contact when thin shell element formulations are used. Use of thick shell elements is recommended.
7. Discrete beam elements, simulating 6-DOF springs, were found to better represent the actual behavior of geocell observed in laboratory testing. However, a standard laboratory procedure for determining the normal and shear stiffness is needed.

7. Limitations

In this study, many assumptions were made in most of the FE analyses. For instance, the shape of the geocell was rhomboidal, except when compared to laboratory results, which is a close approximation to the actual shape of the geocell in the field. Additional evaluation of the contact model for modeling the interface between geocell and the infill material with the laboratory testing is still needed.

8. Acknowledgement

The authors like to gratefully acknowledge financial support for this project received from Texas Department of Transportation (TxDOT).

9. References

- [1]. Emersleben, A., and Meyer, N., "The use of geocells in road constructions over soft soil: vertical stress and falling weight deflectometer measurements", Proceedings of EuroGeo4 – 4th European Geosynthetics Conference, Edinburgh, Scotland, pp. 7-10, 2008
- [2]. Pokharel, S. K., Han, J., Leshchinsky, D., Parsons, R. L., and Halahmi, I., "Behavior of geocell-reinforced granular bases under static and repeated loads", International Foundation Congress & Equipment Expo, pp. 409-416, 2009.
- [3]. Han, J., Pokharel, S. K., Yang, X., Manandhar, C., Leshchinsky, D., Halahmi, I., and Parsons, R. L., "Performance of geocell-reinforced RAP bases over weak subgrade under full-scale moving wheel loads", *J. of Materials in Civil Eng.*, Vol. 23, No. 11, pp. 1525-1534, 2011.
- [4]. Tanyu, B. F., Aydilek, A. H., Lau, A. W., Edil, T. B., and Benson, C. H., "Laboratory evaluation of geocell-reinforced gravel subbase over poor subgrades", *Geosynthetics International*, Vol. 20, No. 2, pp. 47-61, 2013.
- [5]. Mhaiskar, S. Y., and Mandal, J. N., "Investigations on soft clay subgrade strengthening using geocells", *Construction and Building Materials*, Vol. 10, No. 4, pp. 281-286, 1996.
- [6]. Bathurst, R. J., and Knight, M. A., "Analysis of geocell reinforced-soil covers over large span conduits", *Computers and Geotechnics*, Vol. 22, No. 3, pp. 205-219, 1998.
- [7]. Latha, G. M., Dash, S. K. and Rajagopal, K., "Numerical simulation of the behavior of geocell reinforced sand in foundations." *Int. J. of Geomechanics*, Vol. 9, No. 4, pp. 143-152, 2009.
- [8]. Latha, G. M., and Somwanshi, A., "Effect of reinforcement form on the bearing capacity of square footings on sand." *Geotextiles and Geomembranes*, Vol. 27, No. 6, pp. 409-422, 2009.
- [9]. Han, J., Yang, X., Leshchinsky, D. and Parsons, R., "Behavior of geocell-reinforced sand under a vertical load." *Transp. Res. Rec.: J. of the Transp. Res. Board*, No. 2045, pp. 95-101, 2008.
- [10]. Yang, X. "Numerical analyses of geocell-reinforced granular soils under static and repeated loads", Ph.D. dissertation, The University of Kansas, Lawrence, KS, 2010.
- [11]. Evans, M. D., "Geocell mattress effects on embankment settlements", *Vertical and Horizontal Deformations of Foundations and Embankments*, ASCE, pp. 584-597, 1994.
- [12]. Bortz, B., Hossain, M., Accelerated pavement testing of low-volume paved Roads with geocell reinforcement, Final Report FHWA-KS-14-14, Kansas State University Transportation Center, Manhattan, KS, 2015.
- [13]. Hallquist, J. O., "LS-DYNA theory manual", Livermore Software Technology Corp., Livermore, CA, 2006.
- [14]. Lewis, B. A., Manual for LS-DYNA soil material model 147, Report No. FHWA-HRT-04-095, 2004.
- [15]. Klisinski, M., Degradation and plastic deformation of concrete, Ph.D. dissertation, Polish Academy of Sciences, Institute of Fundamental Technology Research (IFTR) Report 38, 1985.
- [16]. Mehdipour, I., Ghazavi, M., and Moayed, R. Z., "Numerical study on stability analysis of geocell reinforced slopes by considering the bending effect", *Geotextiles and Geomembranes*, Vol. 37, pp. 23-34, 2013.
- [17]. Hegde, A., and Sitharam, T. G., "Joint strength and wall deformation characteristics of a single-cell geocell subjected to uniaxial compression", *Int. J. of Geomechanics*, 04014080, 2014.
- [18]. Leshchinsky, B., and Ling, H. I., "Numerical modeling of behavior of railway ballasted structure with geocell confinement",

Geotextiles and Geomembranes, Vol. 36, pp. 33-43, 2013.

- [19]. Neher, H. P., and Lachler, A., “Numerical modeling of a diaphragm wall production process in Rotterdam compared to monitoring data”, 6th European Conf. on Numerical Methods in Geotechnical Eng., Graz, Austria, pp. 417-22, 2006.
- [20]. Latha, G.M., and Rajagopal, K., “Parametric finite element analyses o geocell-supported embankments”, Canadian Geotechnical Journal, 44(8), pp. 917-927, 2007.